EUROPEAN ORGANIZATION FOR NUCLEAR RESEARCH

CERN-PRE-78-151

SEARCH FOR NEW LONG-LIVED PARTICLES WITH MASSES IN THE RANGE 1.4 TO 3.0 GeV, AT THE CERN ISR

J.C.M. Armitage, P. Benz*), G.J. Bobbink, F.C. Erné,
P. Kooijman, F.K. Loebinger, A.A. Macbeth, H.E. Montgomery,
P.G. Murphy, J.J.M. Poorthuis, L. Rabou, A. Rudge,
J.C. Sens, D. Stork†) and J. Timmer

CERN, Geneva, Switzerland,
Daresbury Laboratory, UK,
Foundation for Fundamental Research on Matter (FOM), The Netherlands,
University of Manchester, UK,
University of Utrecht, The Netherlands.

ABSTRACT

A search has been made at the CERN ISR for long-lived non-annihilating particles of two types: thos which exhibit strong interactions and those which do not (heavy leptons). Invariant cross-section upper limits of 6 nb GeV^{-2} and 1.8 nb GeV^{-2} were measured for these two classes of particles, respectively, for particle masses close to the antideuteron mass. Upper limits are also placed on the production of new particles with masses in the range 1.4 to 3.0 GeV, and invariant cross-sections are quoted for π^-, $\bar{p}$, $\bar{d}$ production. The experiment was performed at $\sqrt{s}$ = 53 GeV with x (= $2p_L/\sqrt{s}$) in the range 0.07 to 0.15 and p_T between 0.08 and 0.16 GeV/c. Antideuterons were identified by annihilation in a 1.4 m^3 scintillation calorimeter.

Geneva - 10 October 1978

(Submitted to Nuclear Physics B)

---

*) Deceased.

†) Now at UKAEA, Culham Laboratory, Abingdon, UK.

1. INTRODUCTION

The search for new particle states, especially in the mass range 1.5 to 3.0 GeV, was stimulated by the discovery of the J/ψ and associated ψ' and χ states. The successful interpretation of these particles as "hidden" charm states led to the prediction of new multiplets of states built up from charmed and non-charmed quarks and antiquarks. These "overt" charm states, D's and F's, were expected to have masses in the 1.5 to 3.0 GeV region, and charmed mesons, for example the $D^{\pm}$ with a mass of 1.87 GeV, have subsequently been found [1]. This mass range was also expected to contain the postulated heavy lepton (τ), whose existence was required in some theories to explain the large value of R, the ratio of total hadronic to muon pair production in e^+e^- annihilation above the charm threshold. Early data concerning anomalous $e\mu$ events [2] have been confirmed [3], and the mass of the heavy lepton is estimated to be $\sim$ 1.8 GeV [3,4].

Both the $D^{\pm}$ and the τ lepton decay with a rate characteristic of the weak interaction, i.e. 10^{-12} sec. Current attempts at a unification of weak and electromagnetic interactions, as well as some experimental indications for the occurrence of multimuon events in cosmic rays, suggest that stable or long-lived particles may exist in this mass range. In the gauge theory of Pati and Salam [5] all integrally charged quarks decay into leptons, with lifetimes ranging from 10^{-13} to 10^{-5} sec depending on selection rules. Glashow [6] postulates a doublet of leptons L^0, $U^{\pm}$, the charged members of which have a lifetime (assuming $M_{L^0} > M_{U^{\pm}}$) of

$$\tau = (10\ \theta^2)^{-1} \left(\frac{M_\mu}{M_{U^{\pm}}}\right)^5 \tau_\mu$$

(M_μ and τ_μ are the mass and lifetime of the μ meson) dependent on the Cabibbo angle θ, i.e. stable if $\theta = 0$ and leptonic decays are suppressed. The unification scheme of Lee and Weinberg [7] implies the existence of the "known" quarks and leptons ("even" fermions) as well as a number of so far undiscovered "odd" fermions, at least one of which must be stable.

Krishnaswamy et al. [8] have found a number of cosmic-ray events with several penetrating, non-showering, tracks with origins close to or in the rock of the Kolar mines. These events may be due to long-lived ($> 10^{-9}$ sec) leptons in the mass range 2.0 to 5.0 GeV, although a two-step process, i.e. pair production of heavy leptons $L^{\pm}$ in the upper atmosphere, followed by $L^- \rightarrow L^0 + \mu^- + \bar{\nu}_\mu$, with a semistable L^0 decaying via a second-order weak interaction, has been advanced [9] as an alternative explanation.

This group has been actively engaged in searches for new particle production at the CERN Intersecting Storage Rings (ISR) [10,11] at centre-of-mass energies of $\sqrt{s}$ = 53 GeV. No new resonances were found in ref. 10, which describes the search for short-lived states of mass 1.0 to 3.5 GeV, whose decay might give rise to structures in the effective mass distribution of the two detected hadrons. In a later experiment [11] we have searched for long-lived states and detected large peaks in the positive and negative mass distributions at 1.87 GeV, which were ascribed to deuteron and antideuteron production. No other particles were detected with masses greater than 2.4 GeV -- the upper limit of the deuteron mass distribution -- and the experiment was able to set upper limits at 90% confidence level on the non-invariant differential production cross-section $d^3\sigma/dp\, d\Omega$ of 2.2 nb/GeV/sr for masses up to 17 GeV.

This present experiment was carried out for two reasons. Firstly, to establish the extent to which the peak in the previous experiment [11], at 1.87 GeV in the negative particle mass spectrum, can be ascribed to antideuterons as opposed to some new long-lived state, where "long-lived" in this context is taken as meaning lifetimes greater than 10^{-6} sec because of the length of the spectrometer, $\sim$ 28 m. Secondly, to reinvestigate the mass range 1.5 to 3.0 GeV with improved resolution.

In order to identify the events in the mass peak at 1.87 GeV, the detected particles were made to interact in a 1.4 m^3 calorimeter. The antideuterons were characterized by the deposition of four nucleon masses of energy, the "annihilation

energy", in addition to their kinetic energy. The mass range 1.4 to 3.0 GeV was investigated by means of improved time-of-flight (TOF) and Čerenkov equipment, with which the background due to the tails of the proton and deuteron mass distributions, which covered a large fraction of this mass range in ref. 11, could be reduced.

The bulk of the data were taken with the spectrometer set to select events with masses in the range 1.4 to 3.0 GeV for the new particle search. These data provided a measurement of the invariant differential cross-section for antideuteron production. Calibration data were also taken, which contained mainly pions and protons, and which permitted a measurement of the invariant cross-section for negative pions and antiprotons at values of x and p_T comparable to those of the antideuteron data.

2. APPARATUS AND EXPERIMENTAL PROCEDURE

2.1 The spectrometer

The apparatus consisted of a small-angle single-arm spectrometer [12] (see fig. 1) mounted on top of ISR beam 1. The momentum selection was provided by a septum magnet (S1) and three "bending" magnets (BM1-3) set for a nominal momentum of 1.8 GeV/c and accepting particles in the range 1.4 to 3.0 GeV/c. The nominal production angle in the laboratory frame was 50 mrad, and particles were accepted between 35 and 65 mrad. Charged particles accepted by the spectrometer were detected in eight scintillation counter hodoscopes (A, B, D, E, F, G, H, I) which provided a trigger for the experiment and also gave TOF information. Three Čerenkov counters ($\check{C}_1$, $\check{C}_2$, $\check{C}_3$) were available to veto fast particles, but only the first two were useful in this present experiment. Counter $\check{C}_3$ was therefore evacuated to reduce multiple scattering losses.

The particle trajectories were reconstructed by nine sets of spark chamber modules with magnetostrictive read-out. For the momentum determination only the last six modules were used in the bending magnet region, which included the minimum amount of scattering material, 0.14 radiation lengths of spark chambers. The

efficiency of the track-fitting routine was 63% for these data. Normalization was carried out by recording luminosity monitor counts [12] event by event. Two criteria were applied to the fitted tracks:

i) tracks reconstructed from four or less than four modules were rejected;

ii) tracks which included a definite "kink" were also rejected. For protons accepted at this setting, the percentage momentum error was $\sigma(p)/p = 2\%$.

An important feature of the equipment for this present experiment was the "annihilation calorimeter" (ANC) which was installed at the back of the spectrometer and which is described in detail in Section 2.2. To maximize the relative difference in energy deposited by an annihilating particle and a non-annihilating particle, this experiment was carried out at a lower nominal momentum than that of the experiment described in ref. 11, namely 1.4 to 3.5 GeV/c as opposed to 4.0 to 10.0 GeV/c.

This reduction in momentum also had the effect of improving the mass resolution by increasing the TOF. The TOF system, described in Section 2.3, was additionally improved by the installation of new hardware -- scintillators and more digitizing channels -- and resulted in a typical mass resolution of $\sigma(M) = 22$ MeV at the proton mass, a factor of 6 better than in ref. 11.

To increase the rejection of antiprotons the Čerenkov counter $\check{C}_2$ was used. This counter, described in Section 2.4, was constructed for this experiment and rejected antiprotons with momenta greater than 1.35 GeV/c. This extended the rejection from the 30 atm ethylene Čerenkov $\check{C}_1$, which was used to veto pions and fast kaons. For the main data-taking, $\check{C}_1$ and $\check{C}_2$ were used to veto pions, kaons, and (anti)protons at the hardware trigger level. To select pions and protons for calibration purposes, $\check{C}_2$ and the combination of $\check{C}_1$ and $\check{C}_2$ could be removed from the veto.

2.2 The annihilation calorimeter

The ANC consisted of six 300 mm thick layers of scintillator with 10 mm of lead between each layer (fig. 2). The total of 24 counters, 12 solid and 12 liquid

scintillators, was arranged so that they presented a total face area of 900 × × 800 mm^2 to the envelope of particles (200 × 500 mm^2) emerging from the spectrometer.

The solid scintillators were constructed from blocks of NE110, with dimensions 400 × 300 × 300 mm, wrapped in aluminium foil and encased in 2 mm thick aluminium light-tight boxes. A truncated pyramid of perspex guided the light onto a 58 AVP photomultiplier tube. The liquid scintillator, NE235, was contained in aluminium tanks, 2 mm thick, of dimensions 300 × 300 × 900 mm. The tanks were lined with polished aluminium plates of 2 mm thickness, and the photocathodes of the 58 AVP tubes were immersed in the upper surface of the liquid scintillator. The lead sheets which were placed after each layer of scintillator were used to convert γ-rays and to increase the interaction probability for the secondaries.

The pulse height from each counter was recorded event by event, and provided information on both the total energy deposited by the particle and also the differential deposition of energy as a function of depth of penetration into the ANC. The relative and absolute calibrations of the counters were provided by minimum ionizing particles, which deposited 60 MeV in each scintillation counter. Special calibration runs were made before and after data-taking, in which the whole ANC was displaced laterally to "illuminate" the outer counters. Also, at regular intervals throughout the main data-taking, special runs were taken with the Čerenkov veto out of the trigger (non-vetoed runs) but with the Čerenkov pattern units recorded on the data tape. These runs provided a continuous monitor and calibration of the ANC as well as of the Čerenkov counters and the TOF system. In the longer liquid scintillation counters the effective light attenuation was also measured and the appropriate correction functions were incorporated in the data analysis.

The ANC presented a total absorption of 240 g cm^{-2}, and of that, approximately 180 g cm^{-2} were "live" (scintillator) the rest being "dead" (lead sheets and scintillation counter containers). This corresponds to $\sim$ 4 absorption lengths for antiprotons of 1.5 GeV/c momentum, and in the radial dimension there was $\sim$ 1 absorption

length, depending on the position of the incoming particle. The absorption lengths have been measured for protons, antiprotons, kaons, and pions, and are shown in table 1 together with values calculated from known total and the absorption cross-sections [13].

2.3 The time-of-flight system

For each event a time measurement was recorded at the position of each of eight counter hodoscopes along the length of the spectrometer, 25 m between the first counter and the last. Six of these counters were viewed by two independent phototubes providing two independent TOF measurements. Most of the TOF distributions exhibited non-Gaussian "tails", starting at about 3σ, due to a second particle entering the spectrometer in the long trigger gate required by the low velocities. To reduce these tails a cut was placed at three standard deviations, typically $\sigma = 0.4$ nsec, on the time difference between the two ends, corrected for the position of the particles in the counter. Events which failed this cut were not rejected but the information from that counter was discarded. Timing constants for each counter were calculated using fast particles (pions) in separate "non-vetoed runs". A linear χ^2 fit was then made to the time difference between the $\beta = 1$ calibration events and the $\beta << 1$ data events. If the χ^2 probability of the fit was less than 0.1% the TOF measurement with the highest contribution to the χ^2 sum was rejected and the fit repeated. This procedure was followed until the χ^2 probability exceeded 0.1% or until the number of counters left in the fit was less than three. In the latter case the event was rejected. All events were put through this procedure and the following cuts were then applied:

i) the fitted value of $1/\beta$ must be within the range accepted by the experimental trigger -- with due allowance for the fitted error.

ii) the fitted error in $1/\beta$ must be < 0.02, corresponding to three standard deviations at the highest momentum accepted for antiproton candidates.

Less than 1% of all events were rejected by these cuts, the majority failing condition (i) with too high a velocity, and being consistent with a fast particle entering the spectrometer during the trigger gate formed by a slow particle.

The mass of the particle was calculated using the measured momentum p, and β, and assuming unit charge:

$$M = p\sqrt{\left(\frac{1}{\beta}\right)^2 - 1}\ . \qquad (1)$$

The mass resolution can be calculated from the known momentum resolution and the fitted error in $1/\beta$. Figure 3 shows that the mass resolution for deuterons is at a minimum for the range of momenta selected by the experiment, and $\sigma(M) = 44$ MeV for $M = 1.87$ GeV. Figure 4 shows the performance of the system in identifying pions, kaons, and protons with momenta in the range 1.5 to 3.0 GeV/c.

2.4 The Čerenkov counters

The ethylene gas Čerenkov ($\check{C}_1$) was operated at 30 atm for the first quarter of the data-taking where it vetoed particles with $\beta > 0.97$ (pions and the fast kaons). For the rest of the data-taking, where it vetoed particles with $\beta > 0.991$ (only the pions), it was operated at 11 atm. The second Čerenkov ($\check{C}_2$) was built specifically for rejecting particles with $\beta > 0.821$, corresponding to antiprotons above 1.35 GeV/c and antideuterons above 2.7 GeV/c. During the first quarter of the data-taking the $\check{C}_2$ counts were recorded on the data tape and a cut was imposed in the software. This provided a sample of data with the possibility of analysing high momentum antideuterons, > 2.7 GeV/c. For the rest of the data-taking $\check{C}_2$ was included in the experimental trigger.

For the $\check{C}_2$ Čerenkov counter a Čerenkov radiator with a refractive index around 1.2 was required. Liquid nitrogen or hydrogen can be used but they need complicated cryostats. The cryogenic problem was avoided by using a liquid freon (octafluorocyclobutane C318) which has a boiling point in excess of 20°C, the ambient temperature in the ISR tunnel, at 1.8 atm, and has a refractive index of 1.217. The radiator cell (fig. 5a) consisted of two planar mirrors 360 mm high and 120 mm

wide, facing each other and bolted onto a 20 mm thick aluminium "window frame". Particles traversed the counter at an angle $\alpha = 35°$ determined from the refractive index (n):

$$\alpha = \cos^{-1} (1/n) ,$$

and chosen so that the Čerenkov light from $\beta = 1$ particles entered the phototube (58 AVP) directly with no reflections. At right angles to the radiator cell was a reservoir tank fitted with a thermistor level detector and filled by distillation.

A threshold curve (fig. 5b) was measured with TOF identified protons [14]. The solid line shows the estimated contribution due to δ-rays, which was corrected for in the data.

2.5 The data

The accepted phase space volume is shown in fig. 6. The acceptance is defined by the momentum selection of the spectrometer, by the Čerenkov counter $\check{C}_2$, and by the trigger gate which accepted only particles with $\beta > 0.55$. The bulk of the data were taken at the 1.8 GeV/c momentum setting with Čerenkov veto and selecting negative particles (table 2). Data were also taken at this setting, selecting positive particles for information on deuteron pulse heights in the ANC. Some additional data were taken at half the nominal antideuteron momentum, with no veto in the trigger to measure the threshold in $\check{C}_2$, and throughout the experiment non-vetoed calibration data were taken, which provided a continuous check on the apparatus.

The data correspond to an integrated luminosity $\int L\,dt$ of 10^{37} cm^{-2} or 3.6×10^{11} interacting protons for the negatives and $\int L\,dt$ of 3×10^{35} cm^{-2} or 1.1×10^{10} interacting protons for the positives. The rate of detection of $\bar{d}$ and d^+ candidates with 25 A beams stored in the ISR was one $\bar{d}$/2.5 hours and one d^+/4 min. The acceptance of the spectrometer was approximately 1.2×10^{-4} GeV sr.

3. RESULTS

3.1 The mass spectra

Figures 7 and 8 show the negative and positive mass spectra obtained using eq. (1) on data taken with the two Čerenkovs in veto. Both show a peak at 1.87 GeV, as in ref. 11, but with a measured width of $\sigma(M) \sim 45$ MeV and with a clean separation between the tails of the (10^4) 10^3 times more numerous (anti)protons, and those of the (anti)deuterons.

From the agreement between the measured and computed mass resolution it can be concluded that no strong second peak is present in the vicinity of 1.87 GeV. For the negatives no events are seen in the range 1.45 to 1.7 GeV and no events with mass greater than 2.05 GeV. Two events near 1.4 GeV are possible $^3He^{--}$ events. For the positives, five events are observed near the triton mass, one near 2.4 GeV, and two near 1.4 GeV. One explanation of these events is the presence of a second particle in the spectrometer, which would destroy the timing information, although the enhancement near the triton mass could be tritons produced by secondary scattering in the beam pipe. The production cross-section for this process is enhanced relative to pp scattering by the presence of many nucleons in the nucleus.

We conclude at this point that outside the 1.87 GeV peaks no new long-lived negative (positive) particle has been observed in 3.6×10^{11} (1.1×10^{10}) pp interactions at $\sqrt{s} = 53$ GeV.

3.2 Analysis of the 1.87 GeV peaks in the mass spectra

In examining the 1.87 GeV peaks, the possibility that some of the events may have been produced by collision of a secondary pion or proton with a nucleus in the vacuum pipe has to be considered. As shown in ref. 11, fig. 4, this would give rise to an apparent asymmetry in the distribution of coordinates of the pp interaction point along the direction of the colliding beams, since the spatial distribution is then the result of a convolution of the angular distribution of the primary $[pp \rightarrow p_s X]$ and the secondary $[p_s + \text{Nucleus} \rightarrow d(\bar{d})X]$ interactions. Figure 9 shows the distribution of reconstructed interaction points. For positives this distribution is indeed asymmetric, suggesting that a large fraction of the

positives originate in the beam pipe. Beam-pipe scattering is also likely to produce multiple hits in the first counters of the spectrometer from the products of the nucleon break-up. Multiple hits destroy the timing information in the counters and produce a background in the mass spectra. For the negatives there is no such asymmetry since the threshold for producing a $\bar{d}$ in a p-nucleus collision is 16 GeV/c, too high for secondaries to contribute significantly. The distribution is broadened with respect to ref. 11 owing to the increased importance of multiple scattering at these low momenta, 1.8 GeV/c as opposed to $\sim$ 6.0 GeV/c. In the data a cut of $\pm$50 cm was applied around the interaction point.

For the 104 surviving events in the 1.87 GeV mass peak for negatives, we now ask how many have annihilated in the ANC and can therefore be identified as antideuterons. No corresponding test can be made for the positives, and for lack of evidence to the contrary they are ascribed to deuterons.

In the ANC, particles lose approximately 60 MeV per scintillator block owing to ionization loss, and can also lose part or all of their energy by nuclear interactions. In the latter cases a considerable fraction of the available energy E_{av} goes into neutrals or escapes through the sides of the calorimeter. The observed energy E_0 is thus a fraction ε of the available energy E_{av} and this fraction is energy dependent:

$$\varepsilon(E_0) = E_0/E_{av} \ . \qquad (2)$$

The available energy is related to the known total energy $E = (p^2 + M^2)^{1/2}$, where M is the particle mass, through

$$E_{av} = E - Bm \ , \qquad (3)$$

where B is the baryon number and m is the nucleon mass. Figure 10 shows the measured dependence of ε on E_0 using TOF identified π's, K's, p's, and $\bar{p}$'s. The solid curve is a fit to the data. In this calibration the last layer of the ANC was set to veto the event to ensure that the particles had interacted in the ANC. It can be seen from fig. 10 that ε drops rapidly to a near constant value of 22%. No significant dependence on particle type is seen.

The procedure for identifying particles is the following. For each event we deduce E_0 from the sum of the pulse heights in the ANC. From the curve in fig. 10, ε can be found, and hence E_{av} ($= E_0/\varepsilon$). If the particle is a $\bar{d}$ we expect from eq. (3)

$$E_{av} = (p^2 + 4m^2)^{1/2} + 2m = T + 4m \; ; \quad T = \text{kinematic energy} .$$

Defining the excess annihilation energy as

$$E_{exc} = E_0/\varepsilon - T , \tag{4}$$

we expect E_{exc} to be distributed around the value $E_{exc} = 4m$.

Events due to a long-lived strongly interacting but non-annihilating (i.e. d^+-like) baryon would have

$$E_{av} = (p^2 + 4m^2)^{1/2} - 2m = T$$

and would be distributed around

$$E_{exc} = 0 .$$

Events due to a long-lived strongly interacting baryonium-type $\bar{p}n$ state would have

$$E_{av} = (p^2 + 4m^2)^{1/2} = T + 2m$$

and would be distributed around

$$E_{exc} = 2m .$$

Figure 11 shows the distribution of the events in the negative mass peak versus E_{exc}. It has a broad peak clearly centred on the value 4m, indicating that the majority of the events are antideuterons. The same figure also shows the d^+ events to illustrate the distribution obtained from non-annihilating baryons, with $E_{exc} = 0$. In the distribution of the negatives there is a small excess near $E_{exc} = 2m$, suggesting that some of the events may alternatively be interpreted as

due to a long-lived $\bar{p}n$ state. A few events lie near $E_{exc} = 0$ and are compatible with the non-annihilation hypothesis.

The following points should be noted in relation to fig. 10.

i) Since the efficiency curve $\varepsilon(E_0)$ was compiled from calibration data where the last layer of the ANC was put in veto, then for consistency the same cut has been applied in the software for the $\bar{d}$ candidates. Out of 104 events, 93 survived this cut, and no systematic change in the distribution was introduced by this procedure.

ii) The $\bar{p}$ annihilation events cannot be used in any way as a check, since the ε curve itself is based on the $\bar{p}$ data.

iii) Because of the small binding energy of the deuteron, it may be argued that the $\bar{d}$ should be considered as a system of $\bar{p}$ and $\bar{n}$, each moving with momentum $\frac{1}{2}p$. In that case we would have

$$E_0^{\bar{p}} = E_0^{\bar{n}} = \frac{1}{2} E_0 \ ,$$

and hence

$$E_{exc} = \frac{E_0}{\varepsilon(\frac{1}{2} E_0)} - T \ , \qquad (5)$$

which differs from eq. (4). The numerical difference is negligible, however, since the bulk of the $\bar{d}$ candidates are situated on the flat part of the $\varepsilon(E_0)$ curve (fig. 10) where

$$\varepsilon(E_0) \approx \varepsilon(\tfrac{1}{2} E_0) \ .$$

3.3 The hypothesis of a long-lived, M = 1.87 GeV, heavy lepton

The previous analysis, based on the energy loss through hadronic showers, has to be modified to be applicable to the heavy lepton case. Energy losses here are due to electromagnetic interactions only, and can be related directly to the pulse heights observed for minimum ionizing particles.

Figure 12 shows a plot of momenta versus observed energy for the negatives, and as a comparison the d^+ events are also shown. The solid curve corresponds to

the energy loss $E_{BB}(M,p)$ in scintillator, computed from the Bethe-Bloch formula for a particle of mass M and momentum p. The turn-over at 2.1 GeV/c is due to particles escaping from the back of the ANC.

We can define again an excess energy,

$$E_{exc} = E_0 - E_{BB}(M,p) \tag{6}$$

where E_0 is the observed energy as before. Events satisfying the heavy lepton hypothesis should cluster around $E_{exc} = 0$. Events which contain decays within the sensitive time of the ANC or which have other interactions will have $E_{exc} > 0$.

Figure 13 shows a plot of the $\bar{d}$ candidates as a function of E_{exc}. Most of the $\bar{d}$ candidates deposit an energy well in excess of that expected for leptons. Furthermore, we have examined in detail the 14 events which lie closest to (including all those below) the Bethe-Bloch value. Each of these events is disqualified from being a heavy lepton, because the pulse height per layer is inconsistent with the computed per-layer losses, because the range of the particle is inconsistent with the momentum, or because the hit distribution indicated an interaction or decay.

3.4 Production cross-sections

In this section we collect the invariant differential cross-sections, obtained from the main data-taking and calibration runs, for π^-, $\bar{p}$, and $\bar{d}$, and compare them with earlier results. For the d^+ data no cross-sections have been computed since the contribution due to vacuum pipe interactions is not well known, even with tight cuts on the interaction region of the colliding protons. The invariant cross-sections have been calculated with the formula

$$E\frac{d^3\sigma}{dp^3} = \frac{E}{\langle p_T\rangle}\ \frac{1}{\phi_{m.c.}}\ \frac{N_{data}}{f_{ac}\ f_{ab}\ f_{dc}}\ \frac{1}{\Delta p_L\ \Delta p_T}\ \frac{1}{\int L\,dt} \tag{7}$$

with

$$\frac{E}{\langle p_T\rangle} = \left[1.0 + \left(\frac{\langle p_L\rangle}{\langle p_T\rangle}\right)^2 + \left(\frac{M}{\langle p_T\rangle}\right)^2\right]^{\frac{1}{2}}, \tag{8}$$

where

N_{data} = number of events per Δp_L, Δp_T bin with $\langle p_L \rangle$, $\langle p_T \rangle$ (GeV/c).

$\phi_{m.c.}$ = azimuthal range of Monte Carlo generated events.

f_{ac} = Monte Carlo computed acceptance.

f_{ab} = absorption factor.

f_{dc} = decay factor (pions only).

$\int L\, dt$ = integrated luminosity (cm^{-2}).

The acceptance f_{ac} includes the effects of multiple scattering. The results are listed in table 3. It is seen that the invariant differential cross-section for the production of antideuterons at $\sqrt{s}$ = 53 GeV is of the order of 100 nb GeV^{-2}.

Figure 14 shows a comparison between the π^- and $\bar{p}$ cross-sections of this experiment and those obtained by this group in an earlier (unpublished) measurement. There is good agreement between these results.

Antideuteron production at $\sqrt{s}$ = 53 GeV has previously been studied by Alper et al. (ref. 15), Albrow et al. (ref. 11) and Gibson et al. (ref. 16). The range in $x = p_L/\sqrt{s}$ of the present data, $0.07 < x < 0.10$, is intermediate between the ones of refs. 15 and 16 ($x = 0$) and ref. 11 ($0.18 < x < 0.25$). Assuming a reasonable p_T dependence, there is good internal consistency amongst the data.

The absence of events in the range $1.5 < M < 3$ GeV outside the d^+ and $\bar{d}$ peaks corresponds to the upper limits in cross-section for the production of new particles given in fig. 15. Here we have computed the 90% confidence level limits and taken the mass dependence of the acceptance and multiple scattering into account. We obtain upper limits of 1-2 nb GeV^{-2} for masses in the ranges $m_{\bar{p}} \lesssim M \lesssim m_{\bar{d}}$ and $m_{\bar{d}} < M < 3.3$ GeV; for $M < 1.5$ GeV and $M > 3.3$ GeV the limit rises rapidly because of the limitation in phase space imposed by the equipment (fig. 6).

The absence of non-interacting events in the mass peak at 1.87 GeV for negatives, corresponds to an upper limit for the production of a long-lived negative heavy lepton of M = 1.87 GeV of 1.8 nb GeV^{-2} (90% confidence level). If, instead, we assume the existence of a new, non-annihilating, strongly interacting negative

particle, we obtain a 90% confidence level limit for its production of 6.0 nb GeV^{-2} (fig. 15).

4. CONCLUSIONS

In this experiment we have examined the mass spectrum of long-lived ($\geq 10^{-6}$ sec) or stable negative particles in the range $1.4 < M < 3$ GeV produced inclusively in proton-proton collisions at the CERN ISR. The equipment has a mass resolution in the range $20 < \sigma(M) < 70$ MeV and the ability to recognize antiparticles by their annihilations.

The main conclusions are as follows:

1) No particles other than $\bar{d}$ have been seen in the range $1.5 < M < 3$ GeV, and the 90% confidence level limit for their production cross-section is of the order of 1.5 nb GeV^{-2}. For comparison we note that under similar kinematical conditions ($\sqrt{s}$ = 53 GeV, $p_T \approx 0.15$ GeV, x = 0) the J/ψ production cross-section is approximately [17] 30 nb GeV^{-2}.

2) The particles observed at $M \simeq 1.87$ GeV are all consistent with being anti-deuterons. The upper limit for the cross-section for the production of a heavy lepton of mass 1.87 GeV is 1.8 nb GeV^{-2}. The upper limit for the cross-section for production of a strongly interacting non-annihilating particle of mass 1.87 GeV is 6 nb GeV^{-2}.

3) We have obtained invariant differential cross-sections for the inclusive production of low-momentum π^-, $\bar{p}$, and $\bar{d}$. There is good agreement with other data at $\sqrt{s}$ = 53 GeV in this region of phase space.

After completion of the manuscript two papers have appeared in which searches for long-lived heavy particles are reported. The experiment of Cutts et al. [18] reports a (90% confidence level) upper limit of 1.1×10^{-37} cm^2/GeV^2/nucleon for masses in the range $4 < M < 10$ GeV produced in 400 GeV p-Be collisions at $0 < x < 0.3$ and $p_T = 0.175$ GeV.

The experiment of Vidal et al. [19] reports a (90% confidence level) upper limit of 3×10^{-37} cm^2/GeV^2 for masses in the range $4.5 < M < 6.0$ GeV produced in 400 GeV p-Be collisions at $x = 0$, $p_T = 0$. In both experiments the mass range for which upper limits are obtained is adjacent to the one of the experiment reported here while the negative particles observed around $M \approx 1.9$ GeV have been *assumed* to be antideuterons.

Acknowledgements

We would like to express our thanks to the CERN ISR Division for its support of this experiment. We acknowledge the assistance of Mr. G. Tipler in the construction of the annihilation calorimeter, and of Mr. R. Whitehead for the construction of the freon Čerenkov. We acknowledge the contributions of M.G. Albrow, D.P. Barber, B. Bošnjaković, C.Y. Chang, A.B. Clegg, N.A. McCubbin, D. Radojicic, A.L. Sessoms, J. Singh and P. Strolin to the earlier stages of this experiment. The work was supported in part by the Stichting voor Fundamenteel Onderzoek der Materie (FOM) and in part by the UK Science Research Council through the Daresbury and Rutherford Laboratories.

REFERENCES

[1] I. Peruzzi et al., Phys. Rev. Letters 37 (1976) 569.

[2] M.C. Perl et al., Phys. Rev. Letters 35 (1975) 1489.

[3] W. Bacino et al., Phys. Rev. Letters 41 (1978) 13 and references therein.

[4] R. Brandelik et al., Phys. Letters 73B (1978) 109.

[5] J.C. Pati and A. Salam, Phys. Letters 58B (1975) 333.

[6] S.L. Glashow, Harvard University preprint HUTP-77/A008.

[7] B.W. Lee and S. Weinberg, Phys. Rev. Letters 38 (1977) 1237.

[8] M.R. Krishnaswamy et al., Proc. Roy. Soc. A, 323 (1971) 489.

[9] A. de Rújula et al., Phys. Rev. Letters 35 (1975) 628.

[10] M.G. Albrow et al., Nuclear Phys. B114 (1976) 365.

[11] M.G. Albrow et al., Nuclear Phys. B97 (1975) 189.

[12] M.G. Albrow et al., Phys. Letters 42B (1972) 279.

[13] J.W. Cronin et al., Phys. Rev. 107 (1957) 1121.
R.J. Abrams et al., Phys. Rev. D 4 (1971) 3235.
A. Del Guerra, Nuclear Instrum. Methods 135 (1976) 337.

[14] J. Armitage and G.J. Bobbink, Internal Report, CERN-Holland-Manchester Collab., 21 May 1976, unpublished.

[15] B. Alper et al., Phys. Letters 46B (1973) 265.

[16] V.M. Gibson et al., Nuovo Cimento Letters 21 (1978) 189.

[17] A.G. Clark et al., to be published in Nuclear Phys. B.

[18] D. Cutts et al., Phys. Rev. Letters 41 (1978) 363.

[19] R. Vidal et al., Phys. Letters 77B (1978) 344.

Table 1

Measured absorption lengths (in g/cm^2) for π's, K's, p's, and $\bar{p}$'s

Particle type	Measured	Calculated (σ_{tot})	Calculated (σ_{abs})
Pion	88.0 ± 4.0	58 ± 2	80 ± 4
Kaon	86.0 ± 5.0	59 ± 1	80 ± 1
Proton	79.0 ± 4.0	52 ± 1	76 ± 1
Antiproton	47.0 ± 5.0	29 ± 1	46 ± 1

Table 2

Data taken under several trigger conditions (rounded values)

Trigger veto	Running time (hours)	Integrated luminosity (cm^{-2})	Number of triggers	Momentum range (GeV/c)	Aim
None	12	2×10^{34}	2.3×10^5	1.4 → 3.5	Calibration
$\check{C}_1$ (30 atm),	80	2×10^{36}	6.2×10^5	1.4 → 3.5	$\bar{d}$ search
$\check{C}_1$ (11 atm), $\check{C}_2$	270	1×10^{37}	3.5×10^5	1.4 → 3.5	$\bar{d}$ search
$\check{C}_1$ (11 atm), $\check{C}_2$	10	3×10^{35}	2.7×10^4	1.4 → 3.5	d^+ data
$\check{C}_1$ (30 atm),	2	3×10^{34}	2.5×10^4	0.6 → 2.5	p^+ data
$\check{C}_1$ (30 atm),	3	1×10^{35}	1.7×10^4	0.6 → 2.5	$\bar{p}$ data

Table 3

Invariant cross-sections for $\bar{d}$, $\bar{p}$ and π^-

	$\langle p_L \rangle$	Δp_L	$\langle p_T \rangle$	Δp_T	σ_{inv} ($\mu b\ GeV^{-2}$)
$pp \to \bar{d}X$ $\sqrt{s}$ = 53 GeV	1.75	0.5	0.135	0.01	(16) 0.27 ± 0.07
	1.75	0.5	0.145	0.01	(9) 0.18 ± 0.06
	2.25	0.5	0.135	0.01	(2) 0.07 ± 0.04
	2.25	0.5	0.145	0.01	(9) 0.11 ± 0.04
	2.25	0.5	0.155	0.01	(11) 0.15 ± 0.05
	2.25	0.5	0.165	0.01	(6) 0.12 ± 0.05
	2.75	0.5	0.165	0.01	(6) 0.13 ± 0.05
	2.75	0.5	0.175	0.01	(11) 0.13 ± 0.05
	2.75	0.5	0.185	0.01	(11) 0.28 ± 0.08
$pp \to \bar{p}X$ $\sqrt{s}$ = 53 GeV	1.75	0.5	0.085	0.01	(0.82 ± 0.03) × 10^3
	1.75	0.5	0.095	0.01	(0.94 ± 0.03) "
	2.25	0.5	0.115	0.01	0.82 ± 0.03 "
	2.25	0.5	0.125	0.01	0.95 ± 0.03 "
	2.25	0.5	0.135	0.01	0.99 ± 0.03 "
	2.75	0.5	0.155	0.01	0.81 ± 0.03 "
	2.75	0.5	0.165	0.01	0.93 ± 0.03 "
$pp \to \pi^-X$ $\sqrt{s}$ = 53 GeV	1.75	0.5	0.075	0.01	58.0 ± 2.0 "
	1.75	0.5	0.085	0.01	58.0 ± 2.0 "
	1.75	0.5	0.095	0.01	48.0 ± 2.0 "
	2.25	0.5	0.115	0.01	43.0 ± 2.0 "
	2.25	0.5	0.125	0.01	45.0 ± 2.0 "
	2.25	0.5	0.135	0.01	37.0 ± 2.0 "
	2.75	0.5	0.145	0.01	31.0 ± 1.0 "
	2.75	0.5	0.155	0.01	34.0 ± 1.0 "

Notes

1) In the $\bar{d}$ table the numbers in brackets are the uncorrected numbers of events.

2) For the cross-section calculation only the bins in the centre of the acceptance in p_L, p_T are used. Events in bins, across which the acceptance changes rapidly, have been discarded.

3) Errors quoted are purely statistical.

Figure captions

Fig. 1 : The small-angle spectrometer. S1, BM1, 2, 3 are magnets, $\check{C}_1$ is a high pressure ethylene gas Čerenkov counter, $\check{C}_2$ is a liquid freon Čerenkov counter, $\check{C}_3$ is a gas Čerenkov counter (not used in this experiment); A, B, D, E, F, G, H and I are scintillators. For the annihilation calorimeter (ANC), see fig. 2. The spark chambers have magnetostrictive read-out.

Fig. 2 : The annihilation calorimeter (ANC).

Fig. 3 : The mass resolution as a function of momentum. The full curves indicate the range in β accepted by the trigger.

Fig. 4 : The mass squared spectrum for low-mass particles.

Fig. 5a : The freon Čerenkov $\check{C}_2$.

Fig. 5b : Threshold curve for $\check{C}_2$ using TOF identified protons.

Fig. 6 : The accepted phase space.

Fig. 7 : Mass distribution for negative particles.

Fig. 8 : Mass distribution for positive particles.

Fig. 9 : Distribution of interaction points ("the diamond") for positive and negative particles.

Fig. 10 : The ANC efficiency curve as a function of observed energy.

Fig. 11 : Distribution of events as a function of E_{exc} assuming them to be strongly interacting particles.

Fig. 12 : Scatter plot of energy deposited in the annihilation calorimeter versus momentum, for events in the 1.87 GeV mass peaks. The solid curve has been computed from the Bethe-Bloch formula, i.e. assuming electromagnetic interactions only.

Fig. 13 : Distribution of events as a function of E_{exc} for the heavy lepton hypothesis.

Fig. 14 : Invariant cross-sections for π^- and $\bar{p}$ production in pp collisions at $\sqrt{s}$ = 53 GeV, at fixed angle, i.e. with p_T increasing proportionally to x.

Fig. 15 : 90% confidence level upper limits (solid curve) for the invariant differential cross-section for the production of new long-lived or stable, negatively charged, strongly interacting particles with mass M in the ranges $m_{\bar{p}} \lesssim M \lesssim m_{\bar{d}}$ and $M \gtrsim m_{\bar{d}}$, in pp collisions at $\sqrt{s}$ = 53 GeV, computed from the absence of events in these mass regions. For the events observed in the peak at 1.87 GeV the 90% CL limits for the production of particles other than antideuterons are indicated by arrows, for two assumptions concerning the nature of the particle.

TRIGGERS USED IN THIS EXPERIMENT

(ABDEFGHI) $\overline{\check{C}_1}$

(ABDEFGHI)·$(\overline{\check{C}_1 + \check{C}_2})$

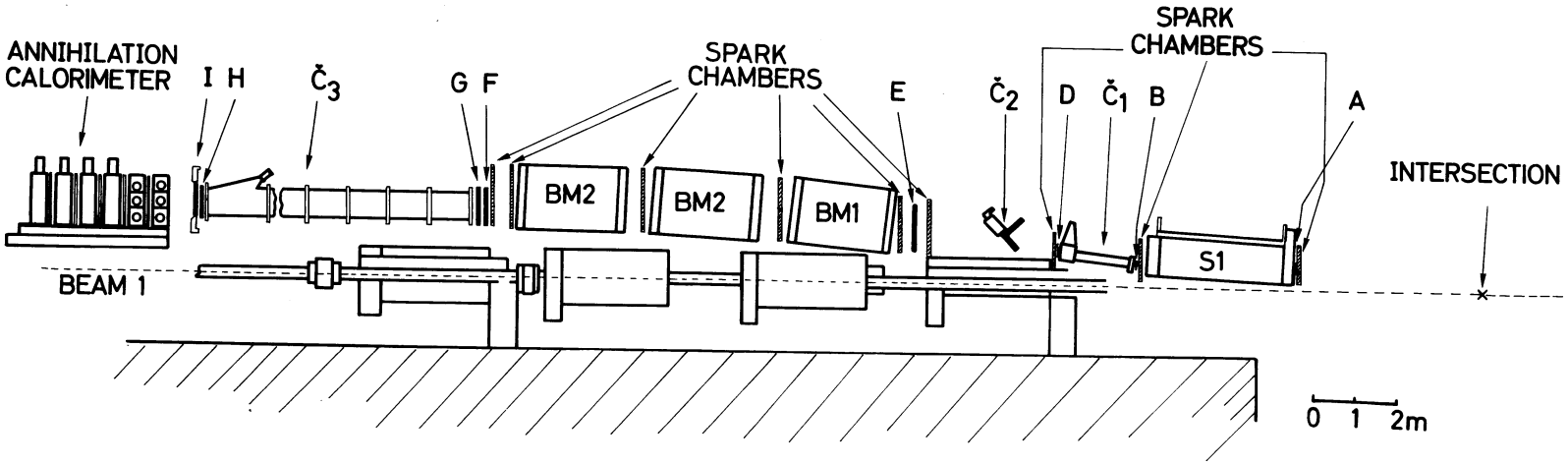

Fig. 1

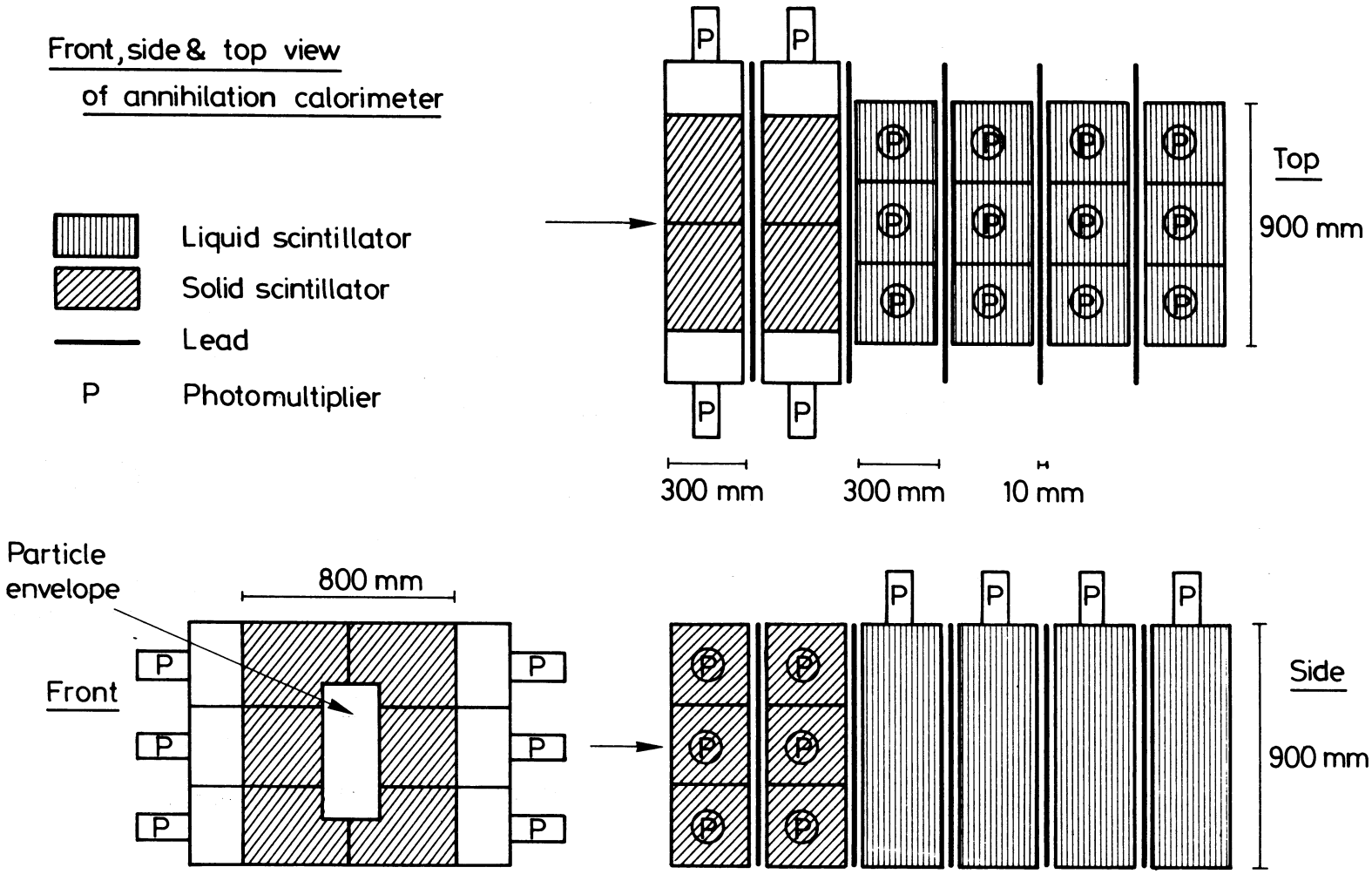
Front, side & top view
of annihilation calorimeter
Liquid scintillator
Solid scintillator
Lead
P
Photomultiplier
Top
900 mm
300 mm
300 mm
10 mm
Particle
envelope
800 mm
Front
Side
900 mm

Fig. 2

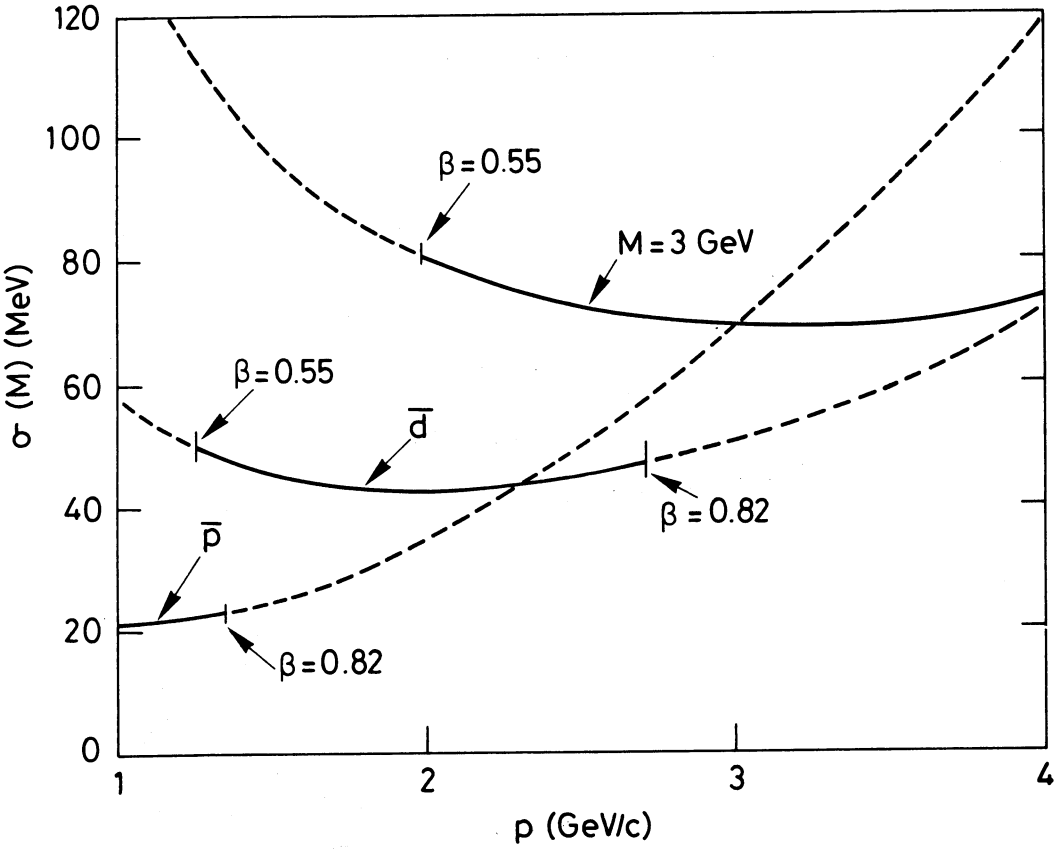
120
100
80
60
40
20
0
σ (M) (MeV)
β = 0.55
M = 3 GeV
β = 0.55
d̄
β = 0.82
p̄
β = 0.82
1
2
3
4
p (GeV/c)

Fig. 3

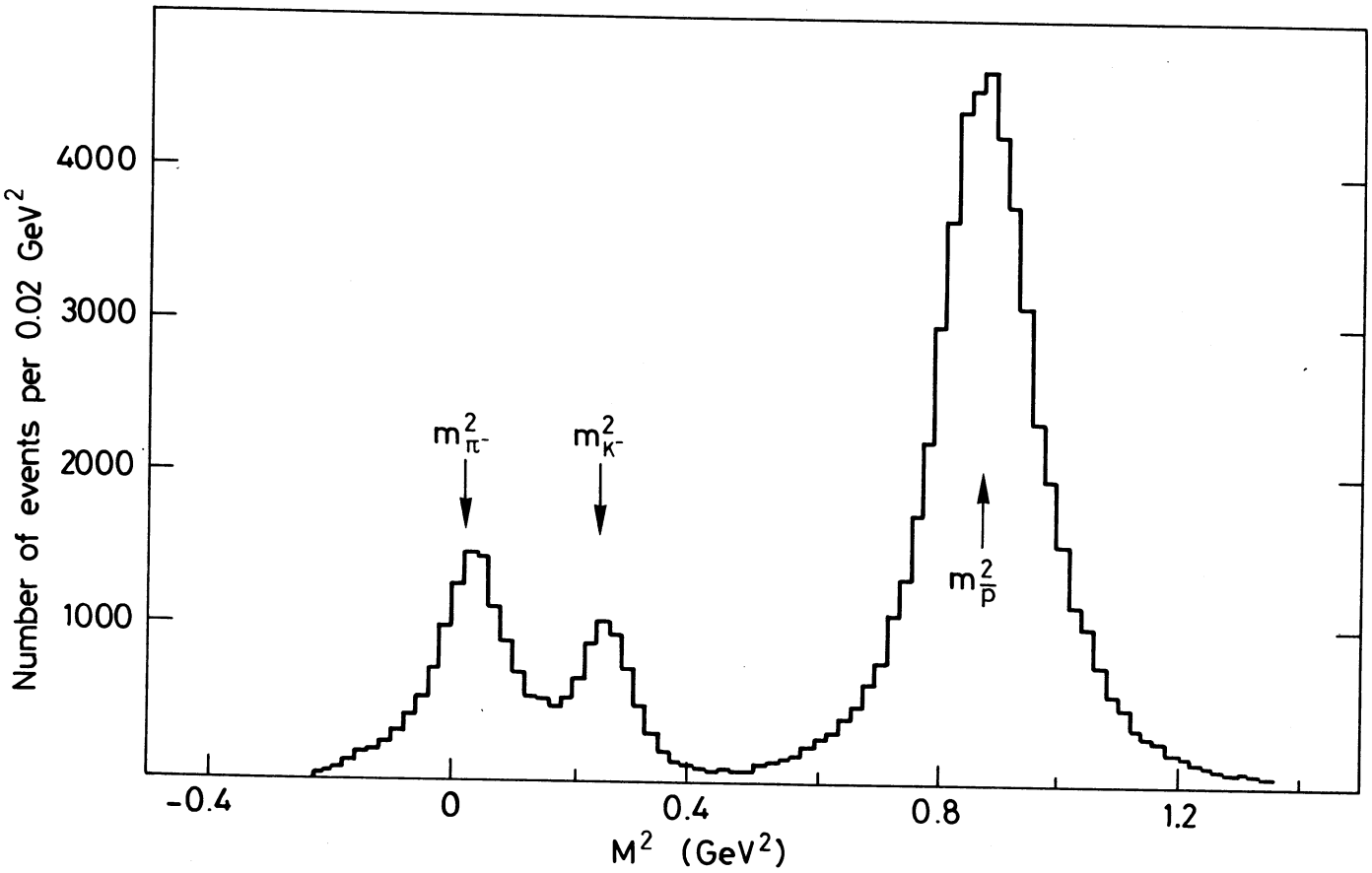
Number of events per 0.02 GeV^2
4000
3000
2000
1000
$m^2_{\pi^-}$
$m^2_{K^-}$
$m^2_{\bar{p}}$
-0.4
0
0.4
0.8
1.2
M^2 (GeV^2)

Fig. 4

a)

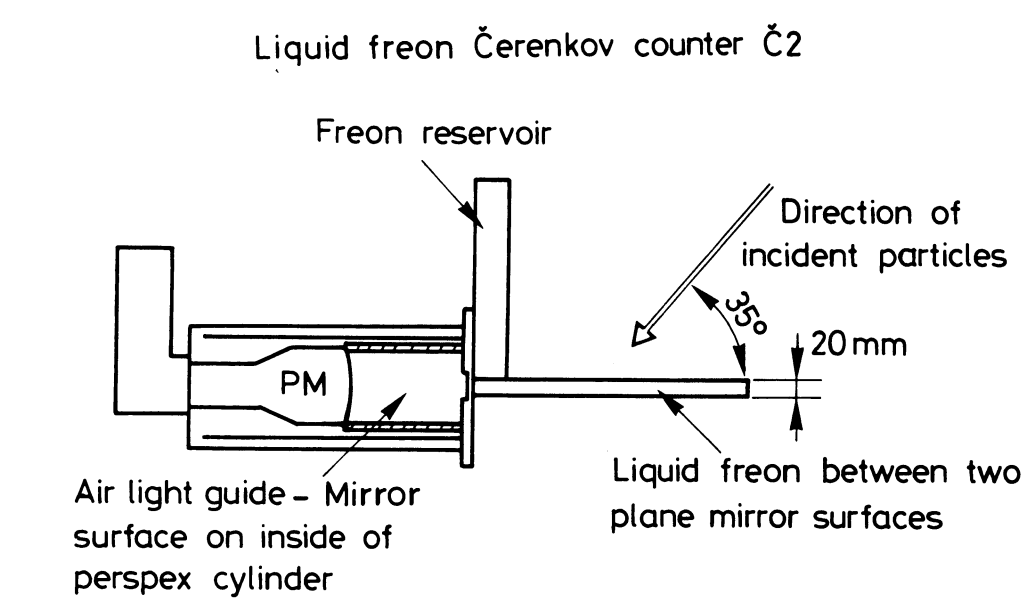
Liquid freon Čerenkov counter Č2
Freon reservoir
Direction of incident particles
35°
20 mm
PM
Air light guide – Mirror surface on inside of perspex cylinder
Liquid freon between two plane mirror surfaces

b)

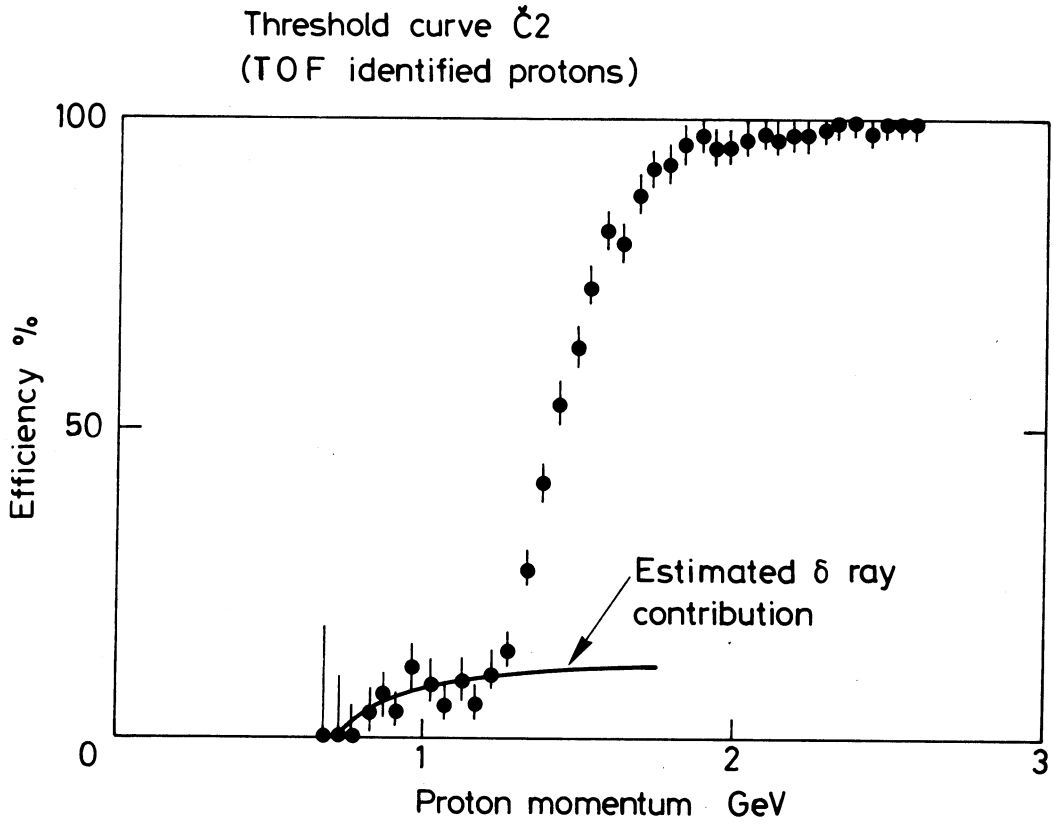
Threshold curve Č2
(TOF identified protons)
100
50
0
Efficiency %
Estimated δ ray contribution
1
2
3
Proton momentum GeV

Fig. 5

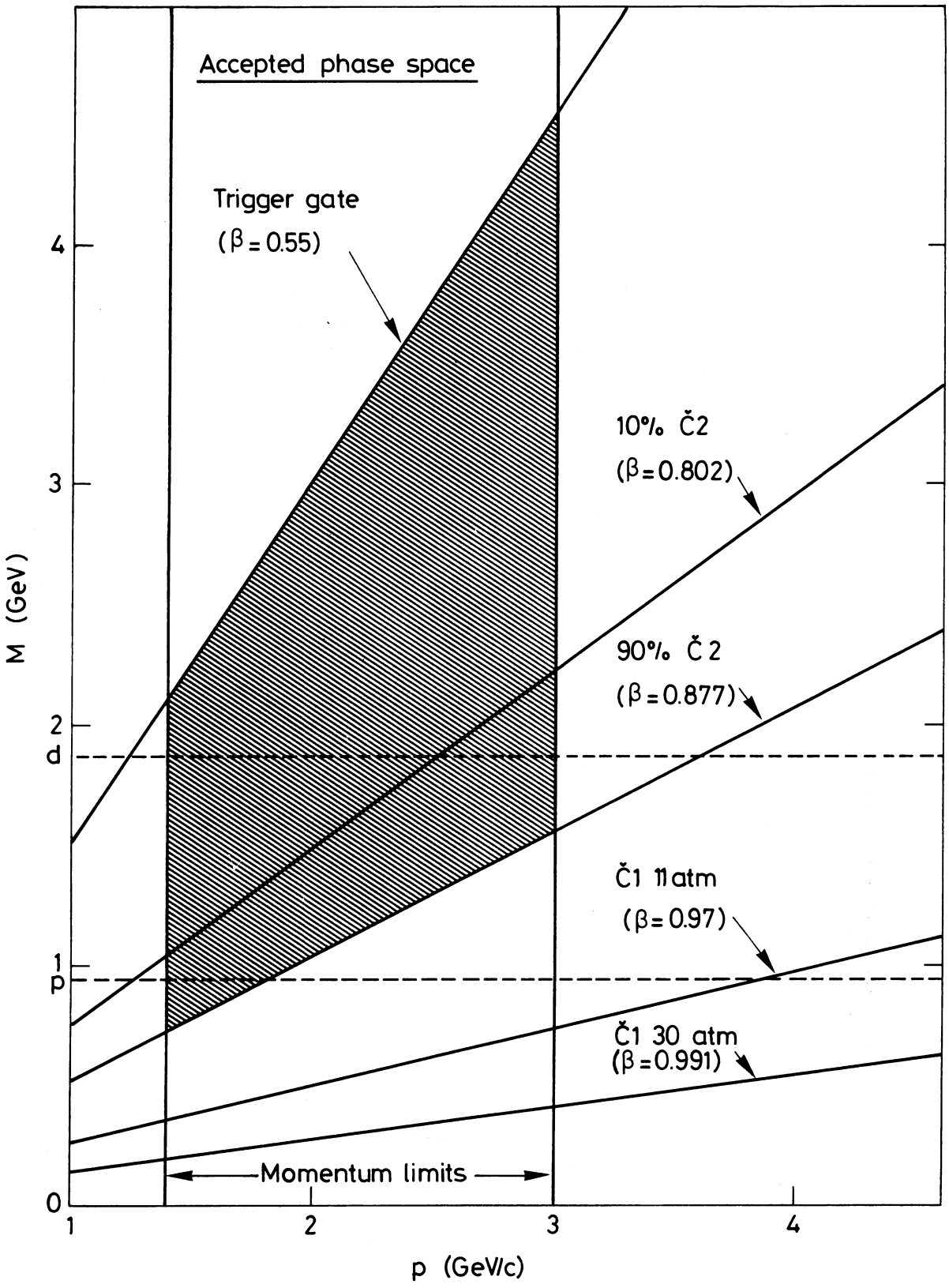
Accepted phase space
Trigger gate
(β = 0.55)
10% Č2
(β = 0.802)
90% Č 2
(β = 0.877)
Č1 11 atm
(β = 0.97)
Č1 30 atm
(β = 0.991)
Momentum limits
M (GeV)
p (GeV/c)
d
p
0
1
2
3
4

Fig. 6

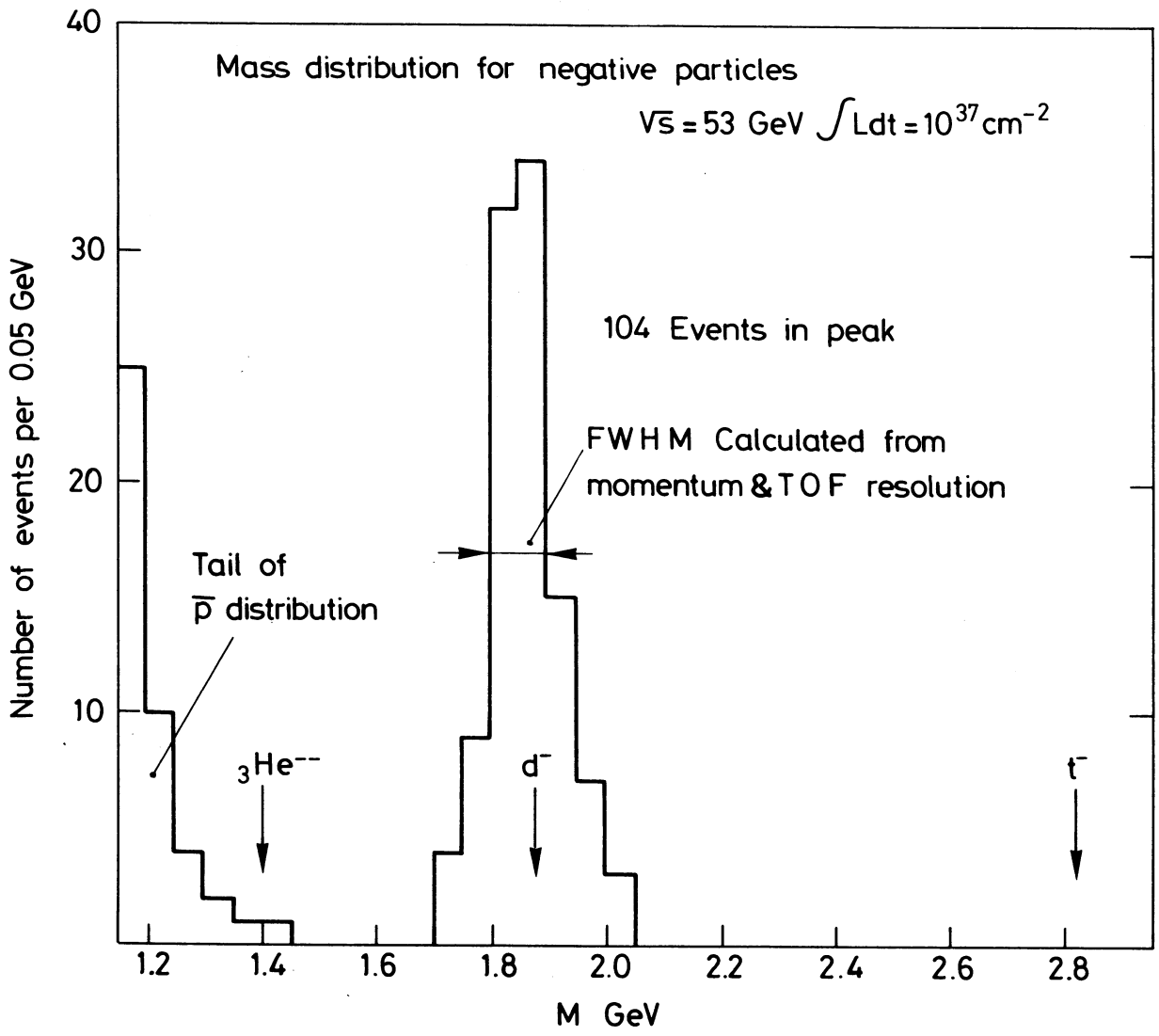
Mass distribution for negative particles
$\sqrt{s}$ = 53 GeV $\int$Ldt = 10^{37} cm^{-2}
104 Events in peak
FWHM Calculated from
momentum & TOF resolution
Tail of
$\bar{p}$ distribution
$_3He^{--}$
d^-
t^-
Number of events per 0.05 GeV
M GeV
40
30
20
10
1.2
1.4
1.6
1.8
2.0
2.2
2.4
2.6
2.8

Fig. 7

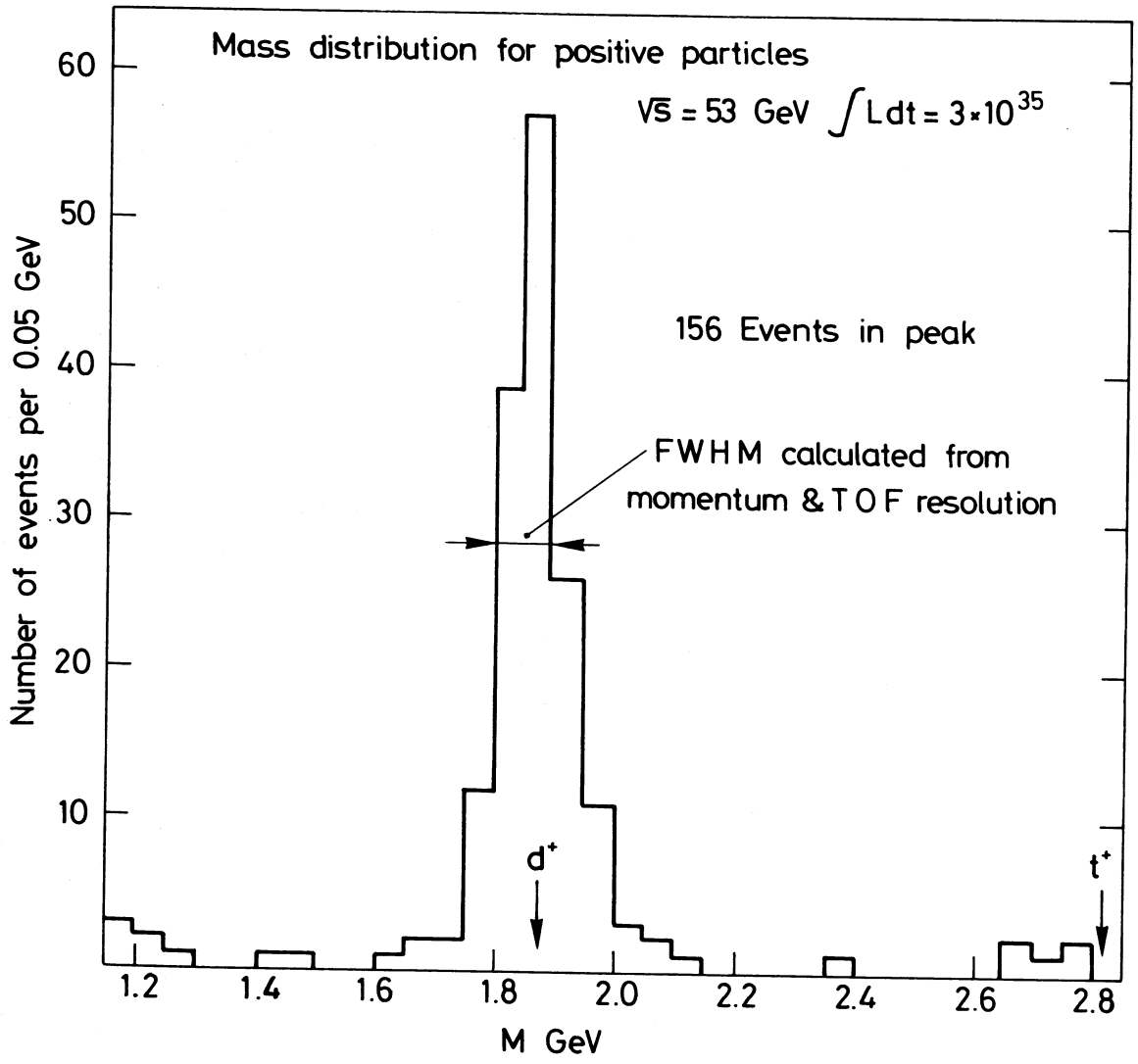
Mass distribution for positive particles
√s = 53 GeV ∫Ldt = 3×10^35
156 Events in peak
FWHM calculated from
momentum & TOF resolution
d+
t+
Number of events per 0.05 GeV
M GeV
60
50
40
30
20
10
1.2
1.4
1.6
1.8
2.0
2.2
2.4
2.6
2.8

Fig. 8

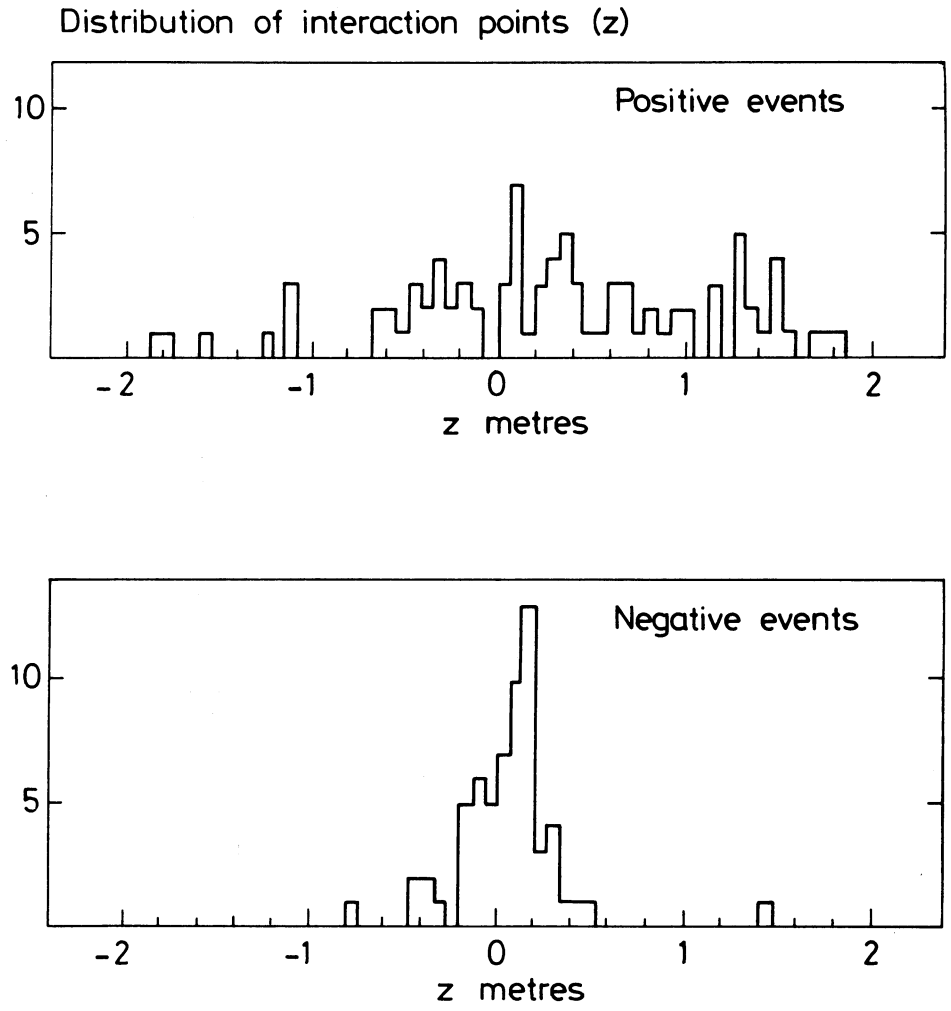
Distribution of interaction points (z)
Positive events
10
5
-2
-1
0
1
2
z metres
Negative events
10
5
-2
-1
0
1
2
z metres

Fig. 9

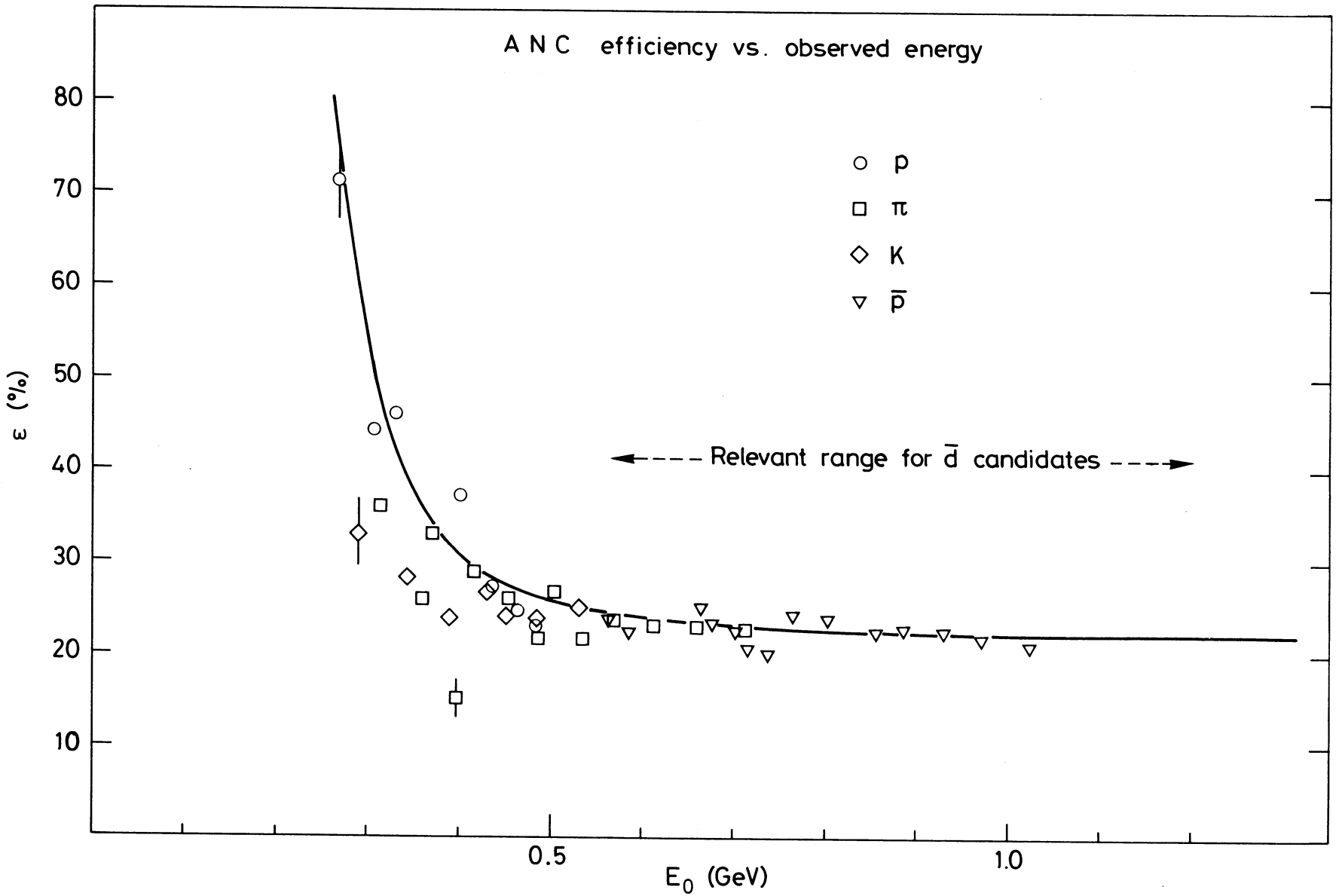
A N C efficiency vs. observed energy
p
π
K
p̄
Relevant range for d̄ candidates
ε (%)
80
70
60
50
40
30
20
10
0.5
1.0
E0 (GeV)

Fig. 10

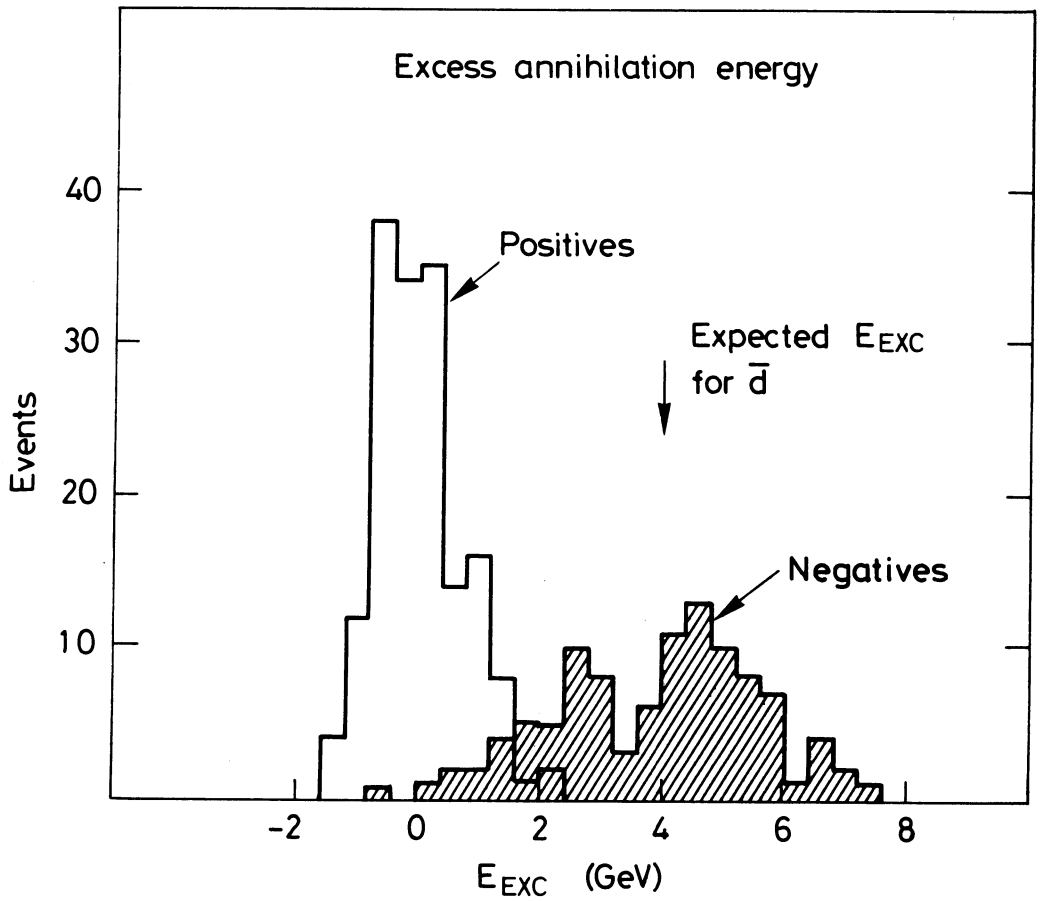
Excess annihilation energy
Positives
Expected E_{EXC} for $\bar{d}$
Negatives
Events
40
30
20
10
-2
0
2
4
6
8
E_{EXC} (GeV)

Fig. 11

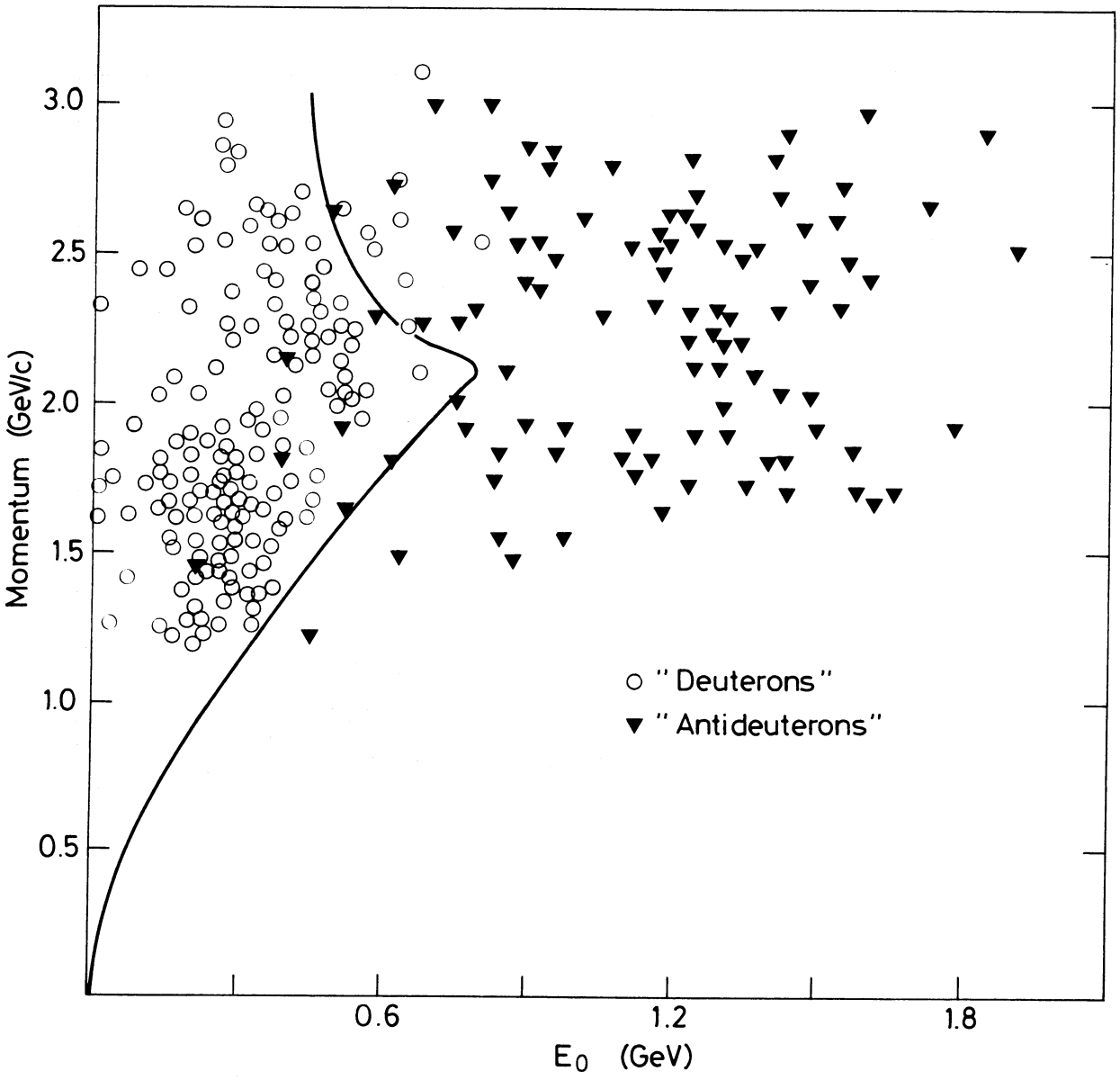
3.0
2.5
2.0
1.5
1.0
0.5
Momentum (GeV/c)
0.6
1.2
1.8
E_0 (GeV)
○ "Deuterons"
▼ "Antideuterons"

Fig. 12

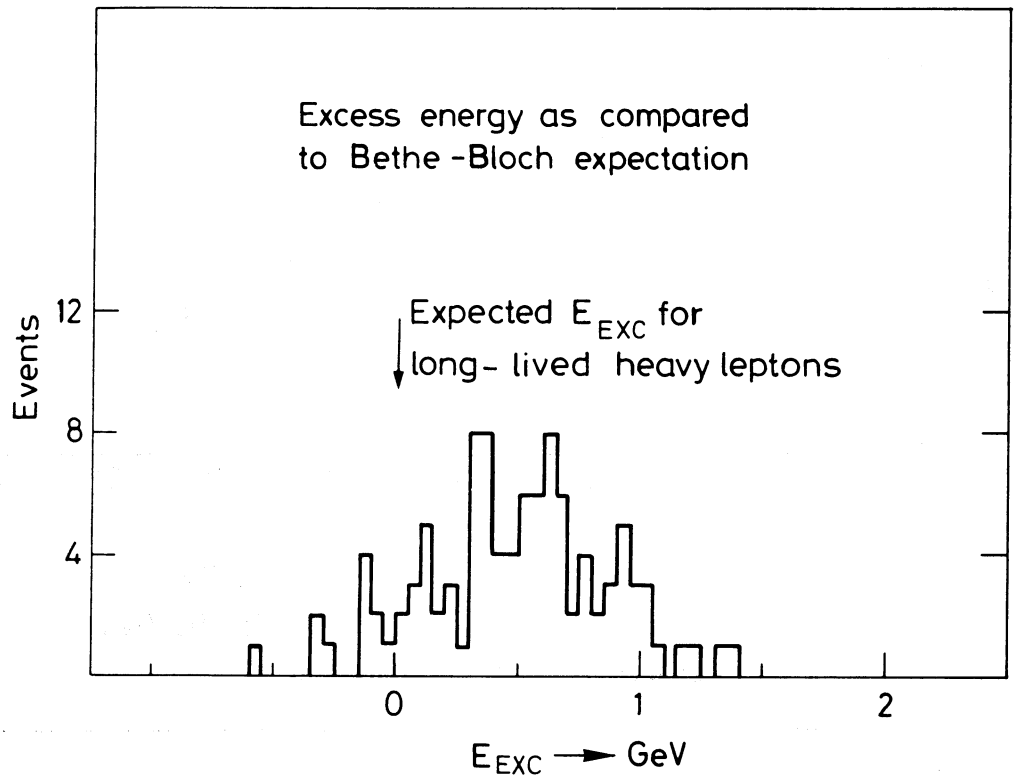
Excess energy as compared
to Bethe -Bloch expectation
Expected E_{EXC} for
long- lived heavy leptons
Events
12
8
4
0
1
2
E_{EXC} → GeV

Fig. 13

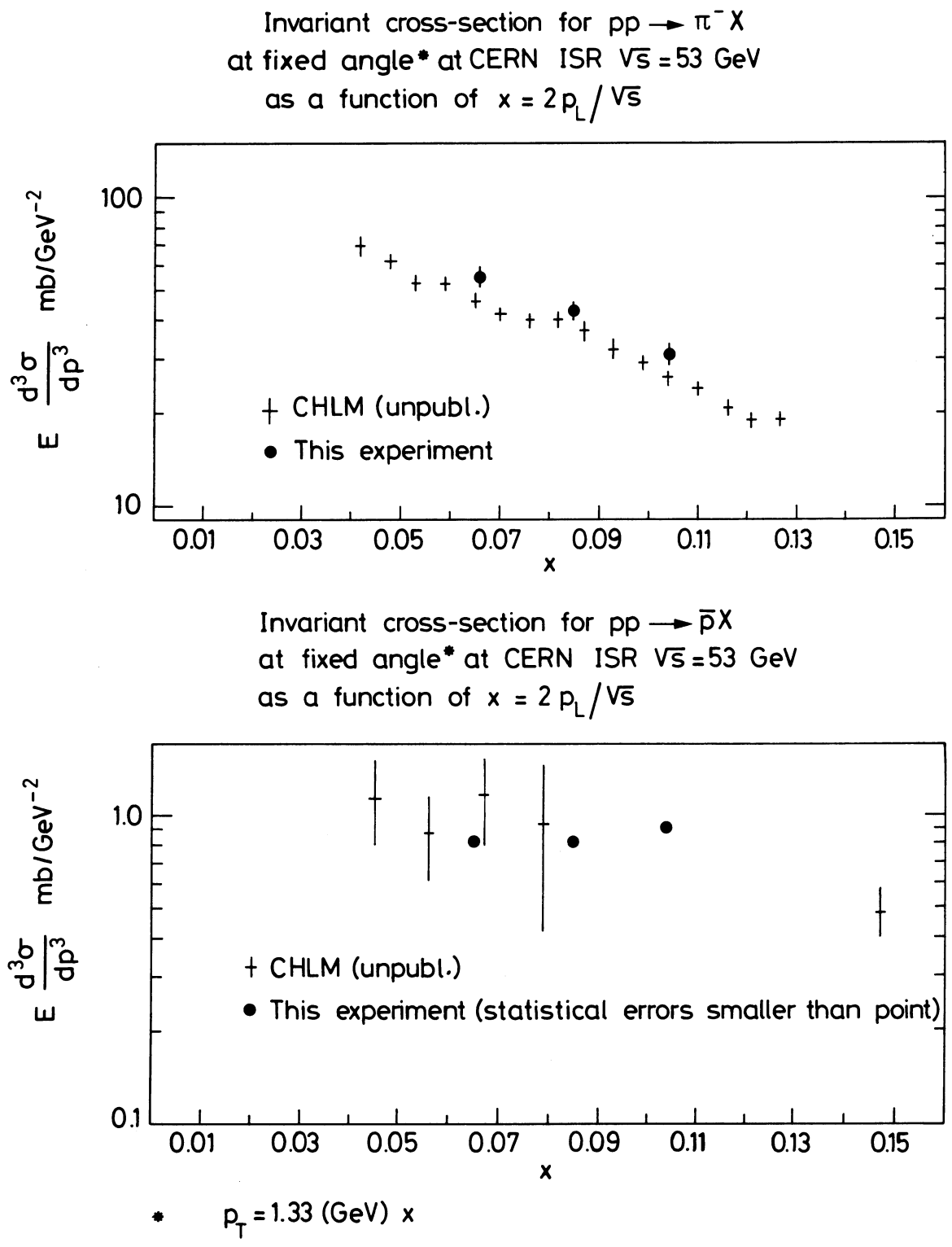
Invariant cross-section for pp → π⁻X
at fixed angle* at CERN ISR √s = 53 GeV
as a function of x = 2p_L/√s
E d³σ/dp³ mb/GeV⁻²
100
10
0.01
0.03
0.05
0.07
0.09
0.11
0.13
0.15
x
+ CHLM (unpubl.)
• This experiment
Invariant cross-section for pp → p̄X
at fixed angle* at CERN ISR √s = 53 GeV
as a function of x = 2p_L/√s
E d³σ/dp³ mb/GeV⁻²
1.0
0.1
0.01
0.03
0.05
0.07
0.09
0.11
0.13
0.15
x
+ CHLM (unpubl.)
• This experiment (statistical errors smaller than point)
* p_T = 1.33 (GeV) x

Fig. 14

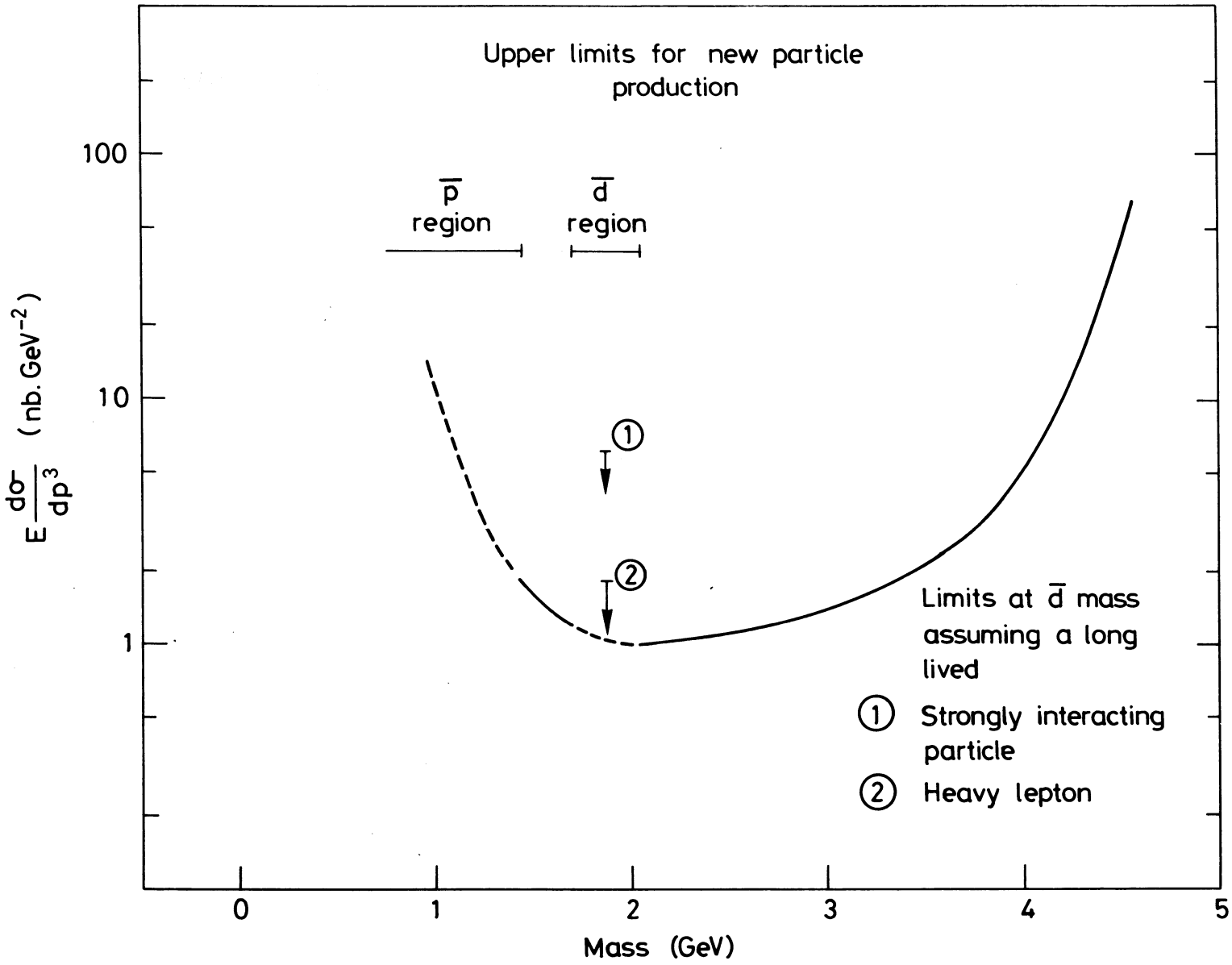
Upper limits for new particle production
100
10
1
$E\frac{d\sigma}{dp^3}$ (nb. GeV^{-2})
$\bar{p}$ region
$\bar{d}$ region
①
②
Limits at $\bar{d}$ mass assuming a long lived
① Strongly interacting particle
② Heavy lepton
0
1
2
3
4
5
Mass (GeV)

Fig. 15